Supporting Information

Promoting OH* adsorption by defect engineering of CuO catalysts for selective electro-oxidation of amines to nitriles coupled with hydrogen production

Xu Yang, Enhui Wei, Yuan Dong, Yu Fan, Hongtao Gao, Xiliang Luo and Wenlong Yang**

X. Yang, E. H. Wei, Y. Dong, Y. Fan, Prof. H. T. Gao, Prof. X. L. Luo, Prof. W. L. Yang

Key Laboratory of Optic-electric Sensing and Analytical Chemistry for Life Science, MOE,

Key Laboratory of Analytical Chemistry for Life Science in Universities of Shandong,

College of Chemistry and Molecular Engineering,

Qingdao University of Science and Technology,

Qingdao 266042, P. R. China

E-mail: xiliangluo@qust.edu.cn; wlyang@qust.edu.cn

Supporting information: DFT calculation method and Figures S1-S12.

Product analysis: Typically, 50 mL of electrolyte was extracted with 50 mL of ethyl acetate after chronoamperometry measurements to probe the oxidation products of benzylamine and determine the Faradaic efficiencies (FEs) at different potentials. The obtained oxidation products were qualitatively and quantitatively analyzed by gas chromatography-mass spectrometer (GCMS-QP2020) using bromobenzene as an internal standard. Meanwhile, a classic water-gas displacing method was utilized to collect the produced H_2 at cathode, which was qualitatively confirmed by gas chromatography.

The FEs for the generation of benzonitrile and H_2 were determined as follows.

$$FE_{benzonitrile}(\%) = \frac{mol\ of\ generated\ benzonitrile}{total\ passed\ charge/4F} \times 100\%$$

$$FE_{H2}(\%) = \frac{mol\ of\ generated\ hydrogen}{total\ passed\ charge/2F} \times 100\%$$

Where F is the Faraday constant (96485 C mol^{-1}).

Calculation Method: Spin-polarized first-principle calculations were performed by the density functional theory (DFT) using the Vienna Ab-initio Simulation Package (VASP) package.[1] The generalized gradient approximation (GGA) with the Perdew− Burke−Ernzerhof (PBE) functional were used to describe the electronic exchange and correlation effects.[2-4] Uniform G-centered k-points meshes with a resolution of $2\pi\times0.05$ $Å^{-1}$ and Methfessel-Paxton electronic smearing were adopted for the integration in the Brillouin zone for geometric optimization. The simulation was run with a cutoff energy of 520 eV throughout the computations. These settings ensure convergence of the total energies to within 1 meV per atom. Structure relaxation proceeded until all forces on atoms were less than 10 meV $Å^{-1}$ and the total stress tensor was within 0.03 GPa of the target value. The DFT+U approach[5] was used to modify the intra-atomic Coulomb interaction among strongly correlated Cu-3d electrons with U_{eff} = 7.14 eV.[6] CuO is a monoclinic structural substance having four Cu and four O atoms in the unit cell that corresponds to the C2/c space group. A supercell of size 2×2×1 was chosen ($Cu_{16}O_{16}$) to calculate its electronic property, and one O atom was removed in the supercell to investigate the effect of O vacancy on its electronic structure.

The averaged adsorption energy of OH^- on V_o-free CuO (111) and V_o-CuO (111) surfaces was calculated by the following equation:

$$\Delta E(ads)=\{E(total)-E(surface)-N*E(OH^-)\}/N$$

which E(total) is the energy of OH^- adsorbed on V_o-free CuO (111) and V_o-CuO (111) surfaces, E(surface) is the energy of V_o-free CuO (111) and V_o-CuO (111) surfaces, $N*E(OH^-)$ is the energy of free OH^-. N is the number of OH^-. The calculated results are listed in Table S1.

The calculated adsorption energy of C_7H_9N on V_o-free CuO (111) and V_o-CuO (111) surfaces was calculated by the following equation:

$$\Delta E(ads)=E(total)-E(surface)-E(C_7H_9N)$$

which E(total) is the energy of C_7H_9N adsorbed on V_o-free CuO (111) and V_o-CuO (111) surfaces, E(surface) is the energy of V_o-free CuO (111) and V_o-CuO (111) surfaces, $E(C_7H_9N)$ is the energy of free C_7H_9N molecule. The calculated results are listed in Table S2.

The calculated desorption energy of C_7H_5N on V_o-free CuO (111) and V_o-CuO (111) surfaces was calculated by the following equation:

$$\Delta E(des) = E(surface) + E(C_7H_5N) - E(total)$$

which E(total) is the energy of C_7H_5N adsorbed on V_o-free CuO (111) and V_o-CuO (111) surfaces, E(surface) is the energy of V_o-free CuO (111) and V_o-CuO (111) surfaces, $E(C_7H_5N)$ is the energy of free C_7H_5N molecule. The calculated results are listed in Table S3.

The dehydrogenation process of from C_7H_9N to C_7H_5N on V_o-free CuO (111) and V_o-CuO (111) surfaces can be expressed as follows:

$$\text{Step1: } * + C_7H_9N \rightarrow C_7H_9N*$$

$$\text{Step2: } C_7H_9N* + OH^- \rightarrow C_7H_8N* + H_2O + e^-$$

$$\text{Step3: } C_7H_8N* + OH^- \rightarrow C_7H_7N* + H_2O + e^-$$

$$\text{Step4: } C_7H_7N* + OH^- \rightarrow C_7H_6N* + H_2O + e^-$$

$$\text{Step5: } C_7H_6N* + OH^- \rightarrow C_7H_5N* + H_2O + e^-$$

$$\text{Step6: } C_7H_5N* \rightarrow * + C_7H_5N$$

where * presents the V_o-free CuO (111) and V_o-CuO (111) surfaces, and intermediates* denotes the corresponding absorbed intermediates.

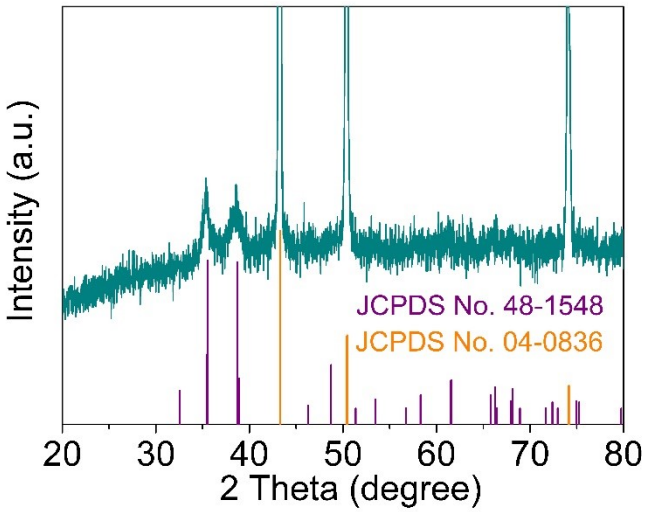

Figure S1. XRD pattern of V_o-rich CuO nanorod arrays on copper foam.

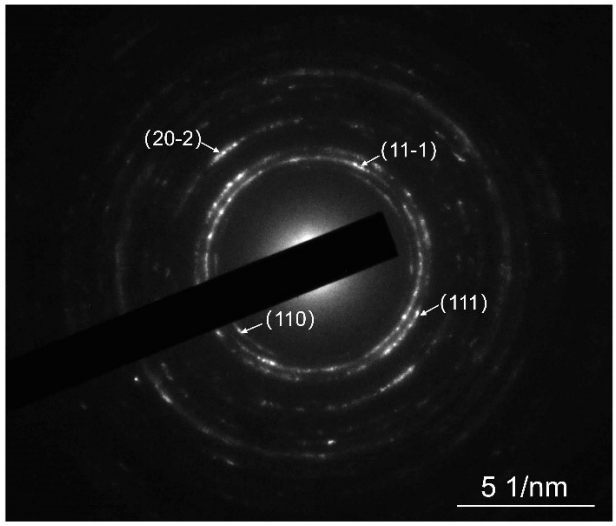

Figure S2. SAED pattern of V_o-rich CuO sample.

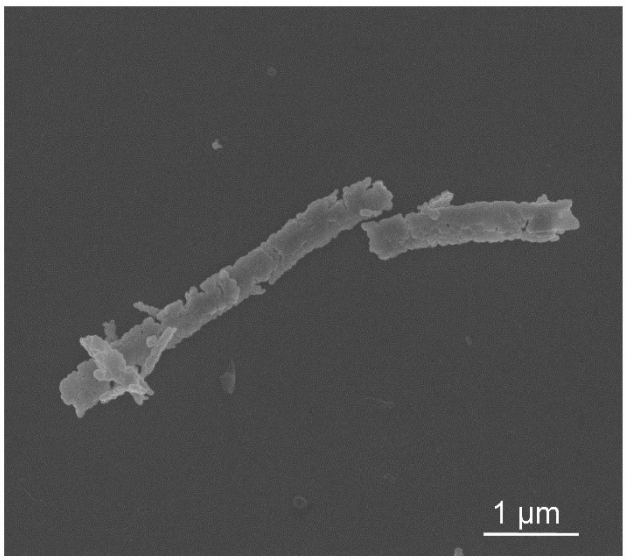

Figure S3. SEM image of V_o-poor CuO sample.

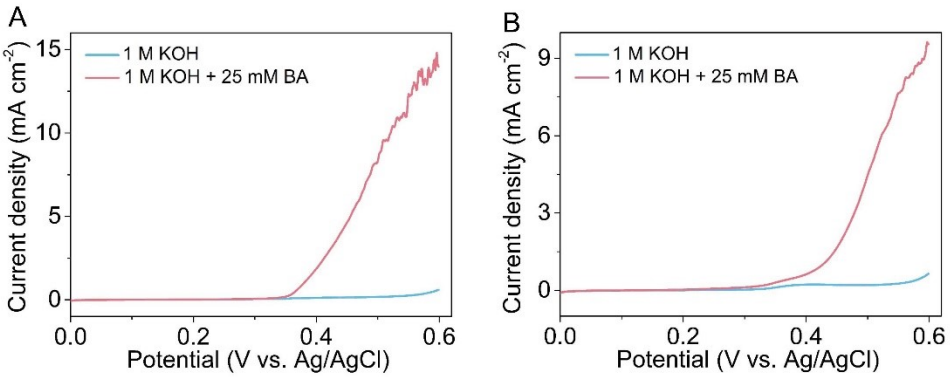

Figure S4. LSV curves of V_o-rich CuO sample (A) and V_o-poor CuO sample (B) in 1.0 M KOH solution with 25 mM benzylamine at a scan rate of 5 mV s^{-1}.

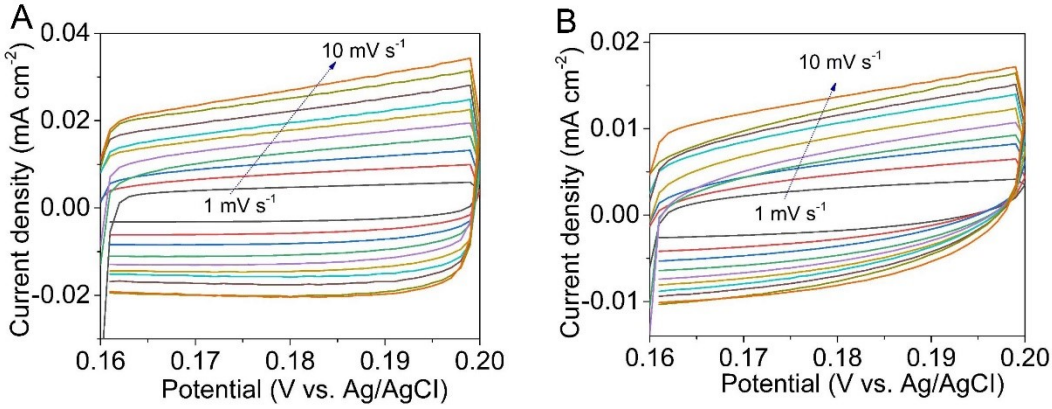

Figure S5. CV curves of V_o-rich CuO sample (A) and V_o-poor CuO sample (B) in 1.0 M KOH solution at scan rates from 1 to 10 mV s^{-1}.

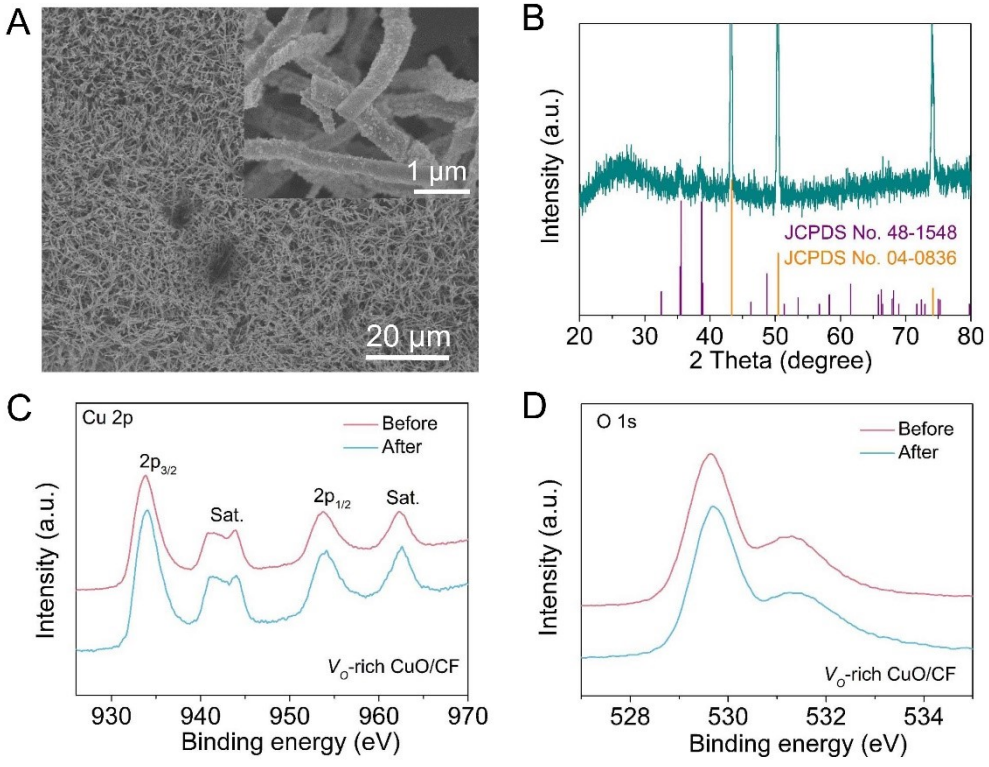

Figure S6. (A) SEM image (inset: enlargement), (B) XRD pattern, (C) Cu 2p and (D) O 1s spectra of V_o-rich CuO/CF after six cyclic tests.

Compared to pristine V_o-rich CuO/CF, the surface of nanorods becomes rougher after six cyclic tests, which is mainly due to the surface reconstruction to CuOOH phase during the electrochemical process.

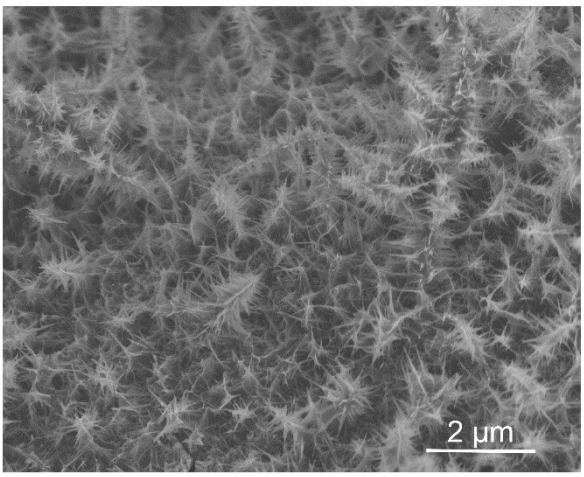

Figure S7. SEM image of NiSe nanorod arrays on nickel foam.

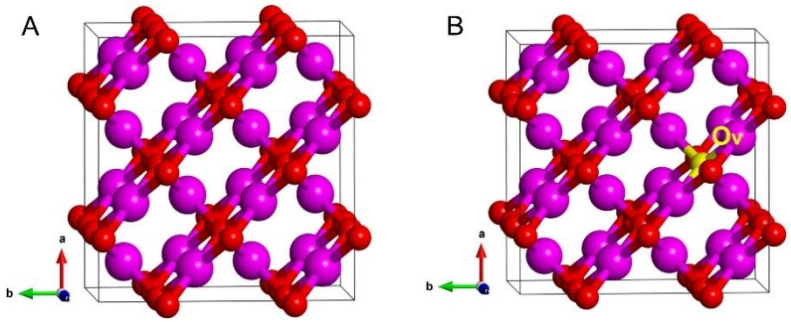

Figure S8. The optimized structures of (A) V_o-free CuO and (B) V_o-CuO. Cu: purple, O: red. The yellow ball denotes the O vacancy.

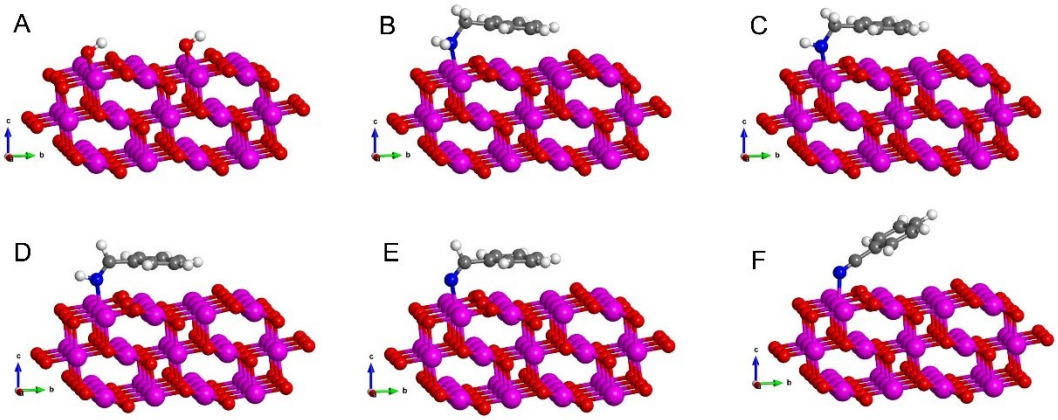

Figure S9. The optimized intermediate structures on V_o-free CuO (111) surface. Cu: purple; O: red; C: black; N: blue; H: white. (A) OH*, (B) C_7H_9N*, (C) C_7H_8N*, (D) C_7H_7N*, (E) C_7H_6N*, (F) C_7H_5N*.

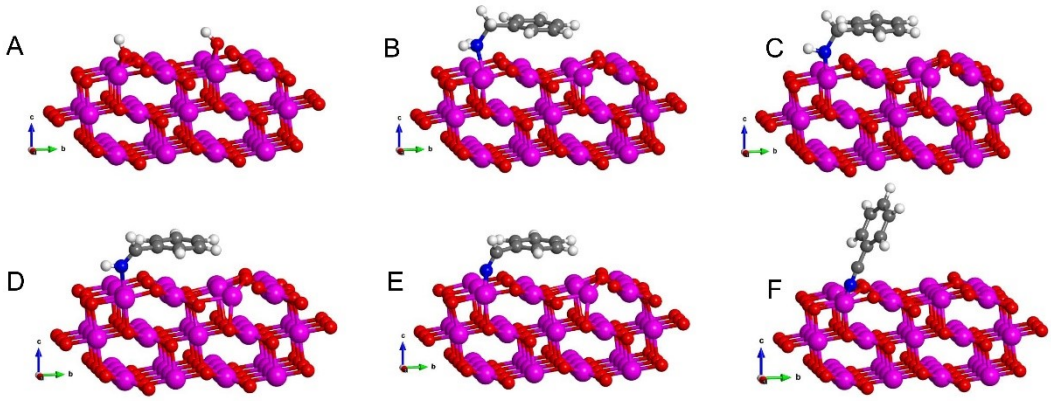

Figure S10. The optimized intermediate structures on V_o-CuO (111) surface. Cu: purple; O: red; C: black; N: blue; H: white. (A) OH*, (B) C_7H_9N*, (C) C_7H_8N*, (D) C_7H_7N*, (E) C_7H_6N*, (F) C_7H_5N*.

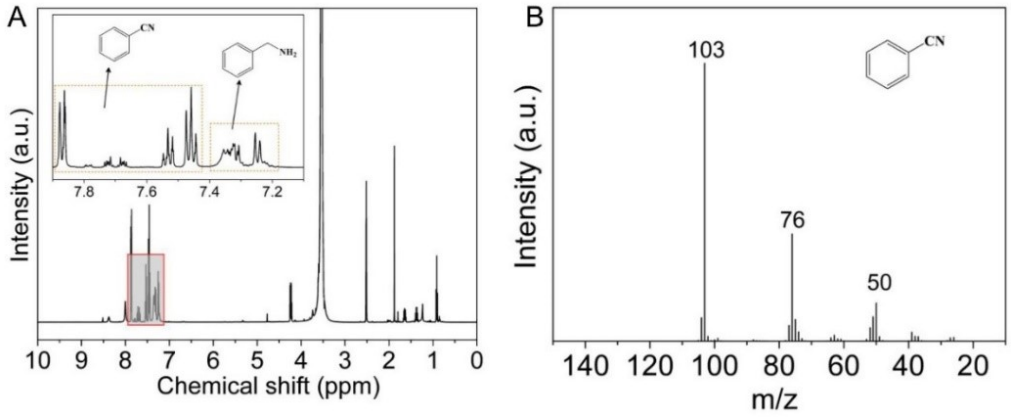

Figure S11. (A) ^{1}H NMR spectra and (B) mass spectra of the collected product after BOR.

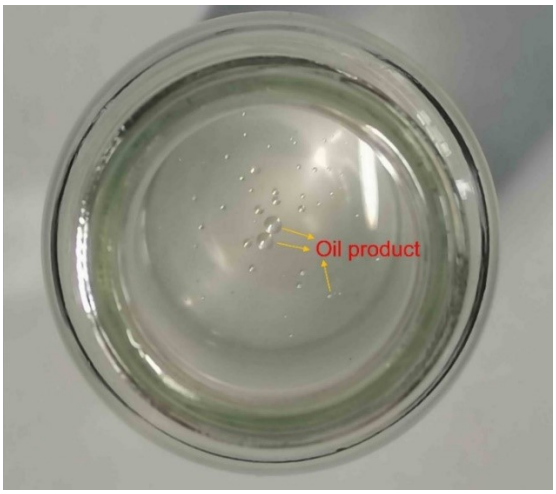

Figure S12. The photograph of oil product floating on the electrolyte surface after 40000 s electrolysis in 1 M KOH containing 50 mM BA.

Table S1. The averaged adsorption energy of OH^- on V_o-free CuO (111) and V_o-CuO (111) surfaces, unit: eV.

Species	E(total)	E(surface)	E(OH^-)	N	ΔE(ads)
V_o-free CuO	-378.52605828	-357.08872785	-10.14921985	2	-0.56944536
V_o-CuO	-365.32995913	-343.33997043	-10.14921985	2	-0.84577450

Table S2 The calculated adsorption energy of C_7H_9N on V_o-free CuO (111) and V_o-CuO (111) surfaces, unit: eV.

Species	E(total)	E(surface)	E(C_7H_9N)	ΔE(ads)
V_o-free CuO	-459.81730963	-357.08872785	-101.90313745	-0.82544433
V_o-CuO	-446.7563077	-343.33997043	-101.90313745	-1.51319986

Table S3 The calculated desorption energy of C_7H_5N on V_o-free CuO (111) and V_o-CuO (111) surfaces, unit: eV.

Species	E(total)	E(surface)	E(C_7H_5N)	ΔE(des)
V_o-free CuO	-445.08694067	-357.08872785	-87.55728913	0.44092369
V_o-CuO	-431.12937445	-343.33997043	-87.55728913	0.23211489

Table S4 The calculated intermediates energies on V_o-free CuO (111) surface, unit: eV.

	CuO						
	E	ZPE	TS	G		ΔG	plot G
surface	-357.08872785	-	-	-357.08872785	*+C_7H_9N	0.00000000	0.00000000
C_7H_9N*	-463.42630963	3.920	0.311	-459.81730963	C_7H_9N*	-0.82544433	-0.82544433
C_7H_8N*	-458.39911183	3.551	0.365	-455.21311183	C_7H_8N*	1.77790364	0.95245931
C_7H_7N*	-455.38679273	3.261	0.359	-452.48479273	C_7H_7N*	-0.09797506	0.85448425
C_7H_6N*	-450.59509540	2.946	0.352	-448.00109540	C_7H_6N*	1.65740317	2.51188742
C_7H_5N*	-447.33494067	2.646	0.398	-445.08694067	C_7H_5N*	0.08786057	2.59974799
H_2O	-14.28351401	0.559	0.671	-14.39551401	*+C_7H_5N	0.44092369	3.04067168
OH^-	-11.56921985			-11.56921985			
C_7H_9N	-104.68613745	3.878	1.095	-101.90313745			
C_7H_5N	-89.19028913	2.636	1.003	-87.55728913			

Table S5 The calculated intermediates energies on V_o-CuO (111) surface, unit: eV.

	CuO						
	E	ZPE	TS	G		ΔG	plot G
surface	-343.33997043	-	-	-343.33997043	*+C_7H_9N	0.00000000	0.00000000
C_7H_9N*	-450.32330774	3.930	0.363	-450.32330774	C_7H_9N*	-1.51319986	-1.51319986
C_7H_8N*	-446.05437640	3.605	0.338	-446.05437640	C_7H_8N*	1.14263718	-0.37056268
C_7H_7N*	-442.26758744	3.265	0.354	-442.26758744	C_7H_7N*	0.60449480	0.23393212
C_7H_6N*	-437.71879708	2.944	0.358	-437.71879708	C_7H_6N*	1.39749620	1.63142832
C_7H_5N*	-433.36737445	2.644	0.406	-433.36737445	C_7H_5N*	1.17712847	2.80855679
H_2O	-14.28351401	0.559	0.671	-14.28351401	*+C_7H_5N	0.23211489	3.04067168
OH^-	-11.56921985			-11.56921985			
C_7H_9N	-104.68613745	3.878	1.095	-104.68613745			
C_7H_5N	-89.19028913	2.636	1.003	-89.19028913			

Table S6. The data of potentiostatic electrolysis at different potentials.

Potential (V vs. Ag/AgCl)	electrolyte	Time (s)	Charge (C)
0.35	70 mL, 1 M KOH+25 mM BA	10000	18.1
0.40	70 mL, 1 M KOH+25 mM BA	10000	89.5
0.45	70 mL, 1 M KOH+25 mM BA	10000	155.4
0.50	70 mL, 1 M KOH+25 mM BA	10000	169.1
0.55	70 mL, 1 M KOH+25 mM BA	10000	183.1

Table S7. Comparison of the electrocatalytic BOR performance between the V_o-rich CuO/CF and recently reported Ni-based catalysts.

Catalyst	Onset potential (V vs. RHE)	FE (%)	Electrolyte
V_o-rich CuO/CF, this work	1.36	93.82	1 M KOH + 25 mM BA
Mn-α-$Ni(OH)_2$[7]	1.31	96	1 M KOH + 25 mM BA
NiSe[8]	1.34	99	1 M KOH + 25 mM BA
Ni_3N[9]	~1.35	~95	1 M KOH + 2 mmol BA
W-doped Ni_2P[10]	~1.32	95	1 M KOH + 25 mM BA
NiFe-MOF/NF[11]	~1.30	99	1 M KOH + 20 mM BA
NiCoFe-CAT[12]	1.29	~87	1 M KOH + 10 mM BA

References

[1] G. Kresse, J. Furthmüller, *Comput. Mater. Sci.* **1996,** *6*, 15-50.

[2] J. P. Perdew, K. Burke, M. Ernzerhof, *Phys. Rev. Lett.* **1996**, *77*, 3865–3868.

[3] P. E. Blöchl, *Phys. Rev. B: Condens. Matter Mater. Phys.* **1994**, *50*, 17953–17979.

[4] G. Kresse, D. Joubert, *Phys. Rev. B: Condens. Matter Mater. Phys.* **1999**, *59*, 1758.

[5] V. V. Anisimov, J. Zaanen, O. K. Andersen, *Phys. Rev. B* **1991**, *44*, 943-954.

[6] M. Jamal, S. S. Nishat, A, Sharif, *Chem. Phys.* **2021**, *545*, 111160.

[7] Y. X. Sun, H. Shin, F. Y. Wang, B. L. Tian, C. W. Chiang, S. T. Liu, X. S. Li, Y. Q. Wang, L. Y. Tang, W. A. Goddard, M. N. Ding, *J. Am. Chem. Soc.* **2022**, *144*, 15185.

[8] Y. Huang, X. D. Chong, C. B. Liu, Y. Liang, B. Zhang, *Angew. Chem. Int. Ed.* **2018**, *57*, 13163.

[9] F. H. Ma, S. H. Wang, L. Y. Han, Y. H. Guo, Z. Y. Wang, P. Wang, Y. Y. Liu, H. F. Cheng, Y. Dai, Z. K. Zheng, B. B. Huang, *ACS Appl. Mater. Interfaces* **2021**, *13*, 56140.

[10] Z. T. Tu, X. Y. He, X. Liu, D. K. Xiong, J. Zuo, D. L. Wu, J. Y. Wang, Z. F. Chen, *Chin. J. Catal.* **2024**, *58*, 146.

[11] K. L. Wei, X. Wang, X. L. Jiao, C. Li, D. R. Chen, *Appl. Surf. Sci.* **2022**, *578*, 152065.

[12] Y. Wang, Y. Y. Xue, L. T. Yan, H. P. Li, Y. P. Li, E. H. Yuan, M. Li, S. N. Li, Q. G. Zhai, *ACS Appl. Mater. Interfaces* **2020**, *12*, 24786.